Matching the metal oxides with a conjugated and confined N-oxyl radical for the photocatalytic C(sp^3)–H bond activation

Ting Li [a],[1], Kaiyi Su [c],[1], Chaofeng Zhang [a],[*], Bingbing Luo [a], Yue Zhang [a], Jinlan Cheng [a], Yongcan Jin [a],[*], Feng Wang [b],[*]

[a] *Jiangsu Co-Innovation Center of Efficient Processing and Utilization of Forest Resources, College of Light Industry and Food Engineering, Nanjing Forestry University, Nanjing 210037, China*
[b] *State Key Laboratory of Catalysis, Dalian National Laboratory for Clean Energy, Dalian Institute of Chemical Physics, Chinese Academy of Sciences, Dalian 116023, China*
[c] *Key Laboratory of Photochemical Conversion and Optoelectronic Materials, Technical Institute of Physics and Chemistry, Chinese Academy of Sciences, Beijing 100190, China*

ARTICLE INFO

ABSTRACT

Generating controllable N-oxyl radicals is an efficient method for the C–H bonds activation. Here the promotion effect of N-hydroxyphthalimide (NHPI) on the photocatalytic C(sp^3)–H bond activation over various metal oxides was systemically studied with control experiments, UV-Vis DRS, FT-IR, ESR, and PCR. Two photocatalytic mechanisms were highlighted for the generation of critical PINO radical from NHPI: (1) The hole oxidation mechanism, the photo-induced hole (h$^+$) of metal oxides directly oxidize the adsorbed NHPI* to a confined PINO*; (2) Ligand-to-metal charge transfer (LMCT) mechanism, the light induces the electron transfer from adsorbed NHPI* to oxides with a wide-band gap and provides a confined PINO*. Furthermore, this work also highlights a lattice-molecular structure matching effect to explain the success of certain oxides in building the h$^+$ oxidation or LMCT systems with NHPI. The corresponding results can inspire further photocatalysis of semiconductors in C–H bond activation with versatile N-oxyl radicals.

1. Introduction

Selective activation of C(sp^3)–H bonds to oxygenated chemicals with O$_2$ as the terminal oxidant is an essential tool in organic synthesis [1–3]. Compared with other mechanisms or strategies, the first activation of the target C–H bond to a carbon radical via a catalytic hydrogen-atom transfer (HAT) mediated by the catalysis of N-oxyl radicals (R$_2$NO•) has drawn much attention in the recent decade [4–13]. The generated carbon radical intermediate can then directly combine with the unreactive $^3\Sigma_g^-$O$_2$ [14], leaving out the complex thermal- or photo-excitation of $^3\Sigma_g^-$O$_2$ to $^1\Delta_g$O$_2$ or other active O* species (Scheme 1A) [15–17], which leads to a relatively controllable and efficient transformation of C–H substrates to oxygenated chemicals under mild conditions. For the in-situ generation of N-oxyl radicals (R$_2$NO•) from various N-hydroxyl compounds (R$_2$NOH) [18–21], most catalytic systems need a trigger process (Scheme 1B) [22–24], which contains

various radical initiators like azocompounds, peroxides, high valence metals, NO$_x$, quinone, or various active oxygen species (O*) after the complex activation of O$_2$. Therefore, it is still an attractive topic to explore simple and green methods for the generation of N-oxyl radicals [25–28]. Furthermore, besides the innovation in generation methods, the topic of regulating the lifetime and activity of one targeted N-oxyl radical has been little focused [5], which is because of the inherent epistemology that N-oxy radicals usually are active free fragments and have a short lifetime [29,30]. If possible, a long-lived and HAT activity-controllable N-oxyl radical is beneficial for the selective C–H bonds activation [31], and the new N-oxy radical generation methods can extend the R$_2$NO• radical chemistry.

As a conjecture, increasing the lifetime of the N-oxyl radical needs to restrain the combination between two N-oxyl radicals or the combination between the N-oxyl radical and its intrinsic radical fragment after molecular rearrangement [22]. Confining the N-oxyl radical on some functional support/catalyst that can also conveniently promote the

generation of N-oxyl radical from N-hydroxyl compounds should be a potential approach (Scheme 1B) [5]. Besides, the different interactions between the adsorbed N-hydroxyl compounds and functional support/catalyst, and the different confining states of the generated N-oxyl radicals may also provide a potential method to regulate the HAT activity of N-oxyl radicals [5,7,9,10]. Therefore, it needs to be considered from the molecular structure level and energy level to reveal this matching relationship between the confined N-oxyl radical and the functional support/catalyst. As a supplementary note, the matching effect needs the organic structure of R_2NOH match well with the anchoring points on the lattice surface of functional support/catalyst, something like Lego building blocks. The structural matching can then provide feasible channels for facilitating the electron transfer to achieve the R_2NOH activation to $R_2NO\bullet$, which needs the precondition that above charge deflection and electron transfer between R_2NOH molecular orbitals and support/catalyst's electronic band structure are permitted [5].

For the potential functional support/catalyst that can achieve the above conjecture, various metal oxide semiconductors are important candidates, which are widely used as photocatalysts in the transformation of organic chemicals [32]. Referring to previous reports, the h^+ of some metal oxides, such as TiO_2 and VO_x [33,34], can directly oxidize the polar ROH/RNH_2 group to RO^+H/RN^+H_2. As an extension, the h^+ of some metal oxides with appropriate valence band potential can achieve the oxidation of R_2NOH to $R_2NO\bullet$ [5], which then promotes the hydrogen abstraction of C–H bonds to carbon radicals. Furthermore, the wide band gap and/or quick recombination of h^+ and e^- are also two limitations for the application of pure metal oxide in photocatalysis under visible light. Based on the extension mentioned above, if the

R_2NOH molecule or $R_2NO\bullet$ radical can match well with the oxide lattice, like two pieces of Lego bricks, the electron interaction between organic groups and semiconductor may enhance the visible light absorption of metal oxide with the mechanism like substrate adsorbing modification [32]. Besides, compared with the photooxidation of free R_2NOH on the heterogeneous oxide surface, the above Lego matching assumption may promote the efficiency of oxidation of R_2NOH to $R_2NO\bullet$ with h^+ consumption, whose effect in another aspect like free photosensitizer to consume the surface h^+ and restrain the quick recombination of photo-generated h^+ and e^- on semiconductors [35]. In our previous work, it was found that commercial α-Fe_2O_3 was one of the desired semiconductor oxides, whose h^+ can directly achieve the photo-oxidation of the adsorbed N-hydroxyphthalimide (NHPI*) to a confined phthalimide-N-oxyl radical (PINO*) that has an unexpectedly long lifetime in seconds magnitude and effectively activates the $C(sp^3)$–H bonds [5].

In this work, the promotion effect of conjugated PINO radical and other potential N-oxyl radicals on the photocatalytic $C(sp^3)$–H bond activation over various metal oxides was further systematically studied. Besides the thermal redox metal mechanism model, three other photocatalytic models, including the electron reduction, the hole oxidation, and ligand-to-metal charge transfer (LMCT) models, were proposed to explain the generation of PINO radical over various metal oxides under the blue LEDs irradiation. In addition, a lattice-molecular structure matching effect hypothesis, including the structure matching between NHPI molecule and oxide lattice surface and following charge deflection and electron transfer between the NHPI molecule orbital and electronic band structure of semiconductors, was highlighted to explain the success of certain oxides in building the h^+ oxidation systems or ligand-to-metal
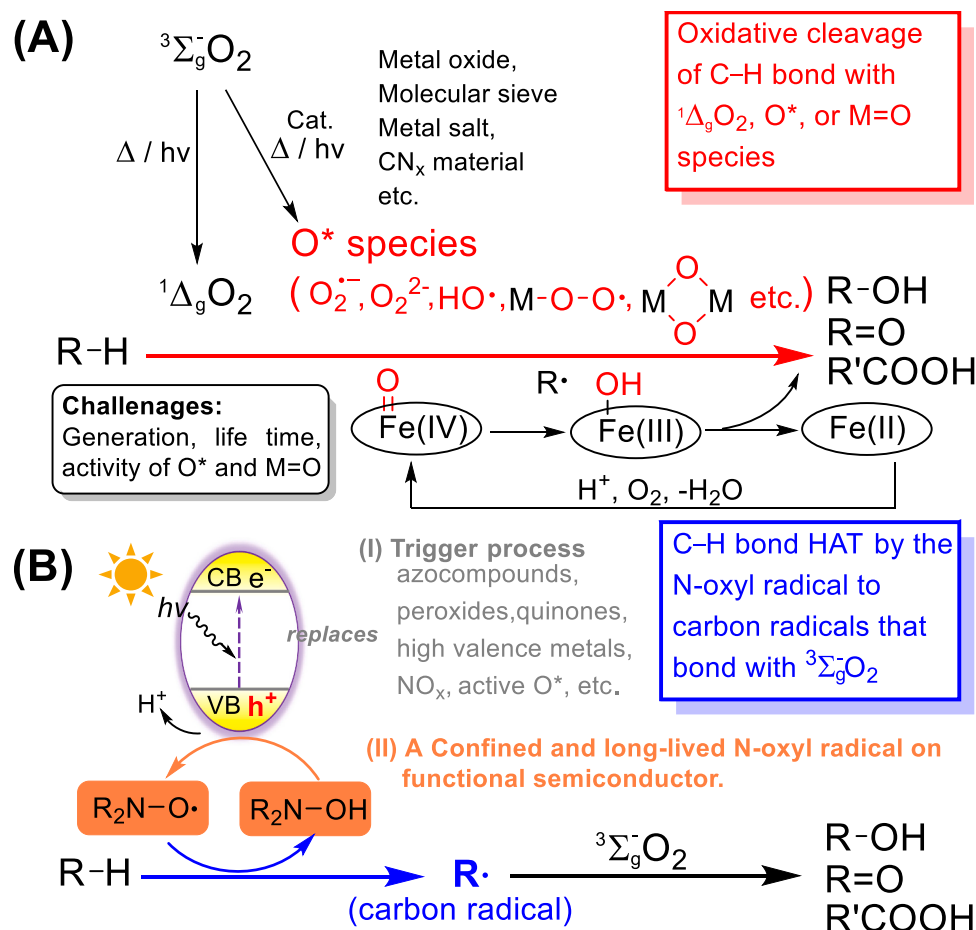
Scheme 1. C–H activation to oxygenated chemicals promoted by active O*(A) and confined N-oxyl radical (B).

charge transfer systems. Furthermore, the kinetic characterization of the confined N-oxyl radical was preliminarily studied with the typical NHPI/α-Fe$_2$O$_3$ system to reveal its difference from the free N-oxyl radical.

2. Experimental

2.1. Chemicals and materials

Acetonitrile, ethylbenzene, other organic chemicals, α-Fe$_2$O$_3$, and other metal oxide nanoparticles were purchased from commercial suppliers without further purifications. The N-hydroxyphthalimide (NHPI) was further recrystallized with ethanol.

2.2. Characterization

The light absorption ability of the metal oxides and their combined mixture with NHPI were analyzed on UV−vis diffuse reflectance spectra, recorded on Shimadzu UV-2600 UV−vis spectrophotometer. The samples of NHPI molecules adsorbed on the metal oxides were obtained from the mixture of metal oxide and NHPI molecules dissolved in acetonitrile solution with a ratio of 30 mg metal oxide, 3 mg NHPI, and 1.0 mL CH$_3$CN, which were further dried in a vacuum oven at ambient temperature. X-ray diffraction (XRD) characterizations were conducted on a Rigaku D/Max 3400 powder diffraction system with Cu Kα radiation (λ = 1.542 Å). Fourier transform infrared spectra (FT-IR) of various KBr tablets were obtained on an Excalibur 3100 spectrometer. To measure the FT-IR results, the samples of NHPI molecules adsorbed on metal oxides were prepared by the addition of a solution of acetonitrile containing NHPI into the metal oxides, which were further desiccated at ambient temperature in the air atmosphere. Electron paramagnetic resonance (EPR) tests were performed on a Bruker spectrometer in the X-band at room temperature with a field modulation of 100 kHz. The microwave frequency was maintained at 9.401 GHz. Typically, 12.5 mg NHPI and 10 mg metal oxide are dispersed in 1.0 mL acetonitrile, then the suspension sample after ultrasonic treatment is enclosed in the quartz capillary tube under Air or Ar atmosphere. The power of the blue LED light (455 nm) for the EPR characterization is 5 W. The photocurrent response (PCR) measurements were conducted on a Bi-Potentiostat CS2350M in a three-electrode system. The catalyst powder (50 mg mL^{-1}) was ultrasonicated in 0.25% Nafion ethanol solution to get a slurry. After that, 30 µL slurry was dispersed onto fluoride tin oxide (FTO) glass with drying treatment at room temperature, and then the side part was protected using sealant 704. The electrodes were immersed in the 0.5 M tetrabutylammonium hexafluorophosphate/acetonitrile solution. The counter electrode and reference electrode were the platinum plate and saturate calomel electrode, respectively. During the measurement, the working electrode was irradiated with a 10 W 455 nm LED light and under an Ar atmosphere. For the metal oxide/NHPI systems, the NHPI (1.0 mg mL^{-1}) was added to the electrolyte solution before the measurement.

2.3. Catalytic reactions and product analyses

Photocatalytic aerobic oxidation of ethylbenzene was carried out in homemade LED photoreactors. Typically, 0.1 mmol of ethylbenzene, 3 mg of NHPI, and 10 mg of catalyst were added to 1.0 mL of acetonitrile in a 10 mL quartz tube, and then the system was replaced with O$_2$. The quartz tube was then irradiated with the 455 nm LED light (6 W). After the reaction, the *p*-xylene as the standard substance in ethanol solution was added to the reaction mixture, after the filtration with a Teflon filter membrane, the products were analyzed by GC-FID (Shimadzu, 2010 Plus) and GC/MS (GC: Shimadzu 2030AM, MS: Shimadzu, QP2020NX).

3. Results and discussion

3.1. The photooxidation activities of various NHPI/metal oxide combinations under the blue LEDs

As the core conjecture of this work is that the combination of semiconductor and N-hydroxyl compounds could be a potential method to adjust the properties of N-oxyl radicals, the promotion effect of conjugated phthalimide-N-oxyl radical (PINO) on photocatalytic C(sp^3)–H bond activation over various metal oxides was first checked. With ethylbenzene oxidation as the model reaction, compared with other listed metal oxides with unobvious photoactivity in the C(sp^3)–H bond, only WO$_3$ NPs can directly mediate the oxidation of ethylbenzene under the blue LEDs (Fig. 1C). The unique property of WO$_3$ NPs in C–H bond photooxidation could be attributed to the generation of the active W–O species under irradiation [36,37] for the HAT process from C–H substrates, which is not obvious for other metal oxides at this mild condition. Then, NHPI as the precursor of the PINO radical is added into the photocatalytic systems (Fig. 1A). Besides the particular case of WO$_3$ which can directly achieve the C–H activation under blue LEDs but has no obvious cooperation with NHPI, referring to the thermal catalytic results of the metal oxide/NHPI systems (Fig. 1B), the promotion effects of NHPI introduction for other metal oxides on the photocatalytic C–H bond activation are in different situations. For the convenience of discussion, the metal oxides in Fig. 1 are marked with different colors. Oxides with red marks, including MnO$_2$, CuO, and Co$_3$O$_4$, have obvious thermal- and photo-oxidation activity in benzylic C–H activation with NHPI. Oxides with blue marks, including Sb$_2$O$_3$, Fe$_2$O$_3$, PbO, Bi$_2$O$_3$, TiO$_2$, Nb$_2$O$_5$, Ta$_2$O$_5$, and Ga$_2$O$_3$, have obvious photocatalytic activity in benzylic C–H bond activation with NHPI. The photoactivity of the metal oxides in black marks is unobvious, and metal oxides in grey marks have no photoactivity with NHPI under blue LEDs. Besides, for the metal oxides in orange marks, such as V$_2$O$_5$, In$_2$O$_5$, MoO$_3$, and NiO, the blue light irradiation can even restrain the thermal activity of the oxide/NHPI systems. In the following discussions, we will mainly focus on the mechanism research of successful photocatalytic systems.

3.2. The relationship between photoactivity and band structure of oxide semiconductors

For the photoinduced reaction, the light harvest is a critical issue for the following photocatalysis, which means that the NHPI, semiconductor, or their combination need to absorb blue light first. Given the fact that the BDE of R$_2$NO–H bond of NHPI in CH$_3$CN is about 368.4 kJ·mol^{-1} (3.82 eV) [40], it is hard for the direct homolysis of R$_2$NO–H bond under 455 nm irradiation (Note: Irradiation peak energy is about 2.72 eV). Referring to the UV-Vis spectrum of NHPI in CH$_3$CN, the light absorption of NHPI alone is not obvious around 455 nm (Fig. S1). However, considering the wavelength distribution of the used LEDs and a trace amount of light with shorter wavelengths may trigger the decomposition of NHPI, but the experimental result shows that the photoactivity of NHPI alone is limited (ethylbenzene conversion ~5%, Fig. 1A). Therefore, to initiate the photoreaction under the blue LEDs, the main resultful light absorption is achieved by the oxide semiconductors or the composited systems of metal oxide/NHPI.

For the light absorption over the metal oxide semiconductors, the band gap is a useful parameter. The metal oxides with a band gap< 2.72 eV that can adsorb the irradiation of the blue LEDs were first checked. While, according to the experimental results from Fig. 1 A and Table 1, the band gap cannot directly determine the photoactivity of the metal oxide/NHPI system. Besides MnO$_2$, CuO, and Co$_3$O$_4$ that have obvious thermal- and photo-oxidation activity in benzylic C–H activation with NHPI, the Sb$_2$O$_3$ and α-Fe$_2$O$_3$ with a band gap below the energy of blue LEDs can cause the obvious photooxidation, but metal oxides like Mn$_3$O$_4$, Cu$_2$O, and CdO with a similar band gap cannot induce the photooxidation. For the other listed metal oxides with a
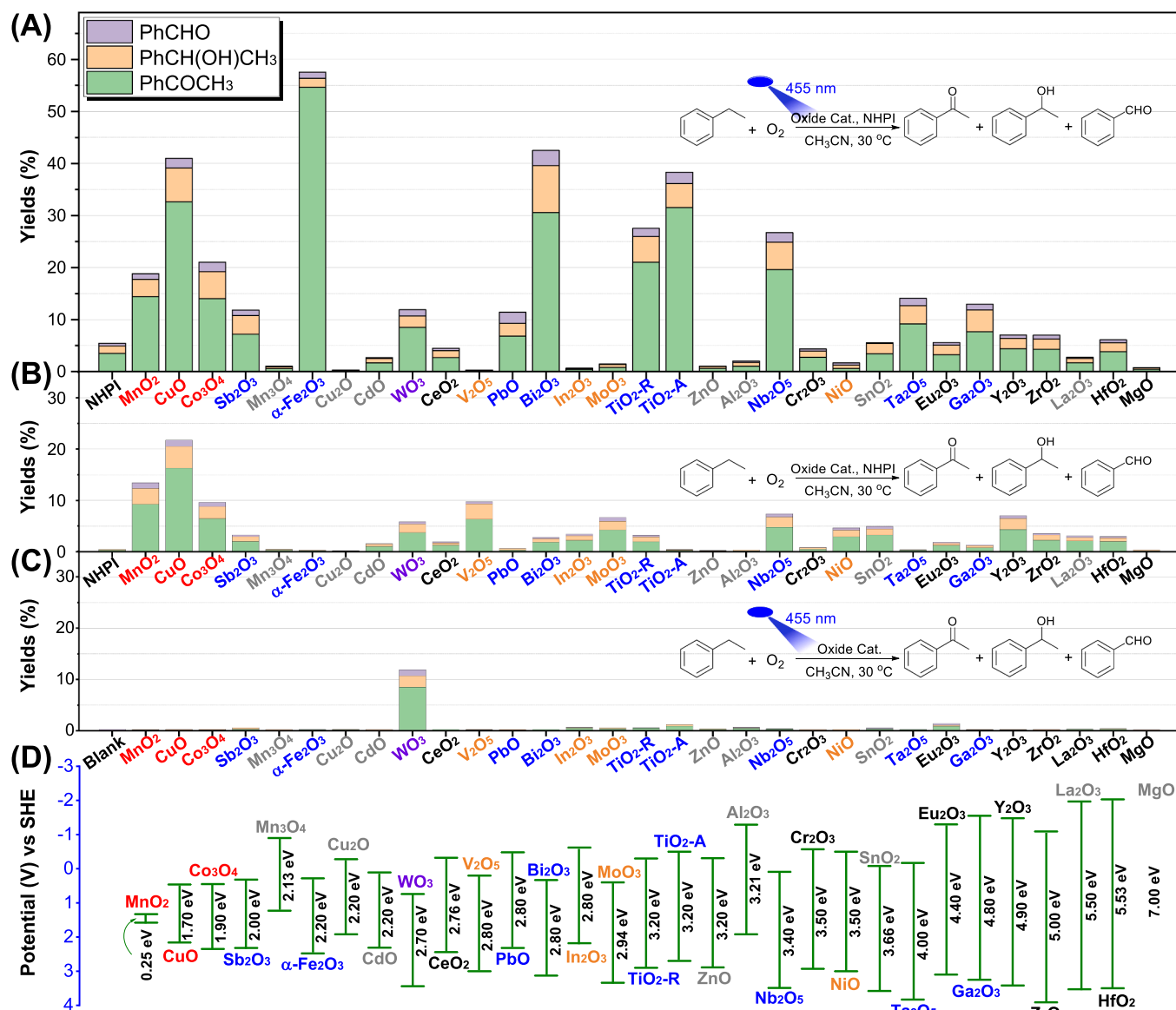
Fig. 1. The photooxidation (A, C) and thermal oxidation (B) activities of various NHPI/metal oxide combinations and just metal oxide systems. Reaction condition: metal oxide 10 mg, ethylbenzene 0.1 mmol, NHPI 3 mg, acetonitrile 1.0 mL, O_2 1 atom, blue LED light (455 nm, 6 W), 30 °C, 10 h. (a) NHPI in Fig. 1A and Fig. 1B means control experiments without metal oxide; (b) Blank in Fig. 1C means control experiments without the catalyst; (c) The absolute energy positions of conduction and valence bands of selected semiconductors in Fig. 1D were abstracted from Schoonen [38]. The MgO has no accurate information on band structure but has a 7.00 eV band gap [39].

larger band gap, above blue light energy (>2.72 eV), the same conclusion is confirmed that the band gap cannot directly determine the photoactivity of the metal oxide/NHPI system. The PbO and Bi_2O_3 showed photoactivity with NHPI, but the oxide like CeO_2, V_2O_5, In_2O_3, or MoO_3 with visible light absorption (> 400 nm, and band gap< 3.1 eV) cannot mediate the photooxidation. Besides, the TiO_2, Nb_2O_5, Ta_2O_5, and Ga_2O_3 can also induce photo-oxidation with NHPI, but other listed metal oxides with the band gap > 3.1 eV in Fig. 1 and Table 1 show unobvious photoactivity with NHPI under the 455 nm irradiation. These phenomena cause our interest to further explore the photocatalytic mechanisms of the metal oxide/NHPI systems from the first light harvest. Next, the light absorption of listed oxides and oxide/NHPI systems (Fig. 1) was measured by the UV-Vis spectrophotometer (Fig. S2–S32 and Table 1). Combined the obtained UV-Vis spectra with the photoactivity of different NHPI/metal oxides systems, it can be concluded that the introduction of NHPI can extend the light absorption of some metal oxides but the irradiation absorption enhancement

around 455 nm cannot always induce the photooxidation with NHPI first dehydrogenation to PINO radical (Table 1 and Fig. 1).

According to previous reports, the oxidation potential of NHPI to PINO radical is about 0.94–1.08 V adjusted relative to NHE [4], most listed metal oxide semiconductors have an appropriate valence band structure (Fig. 1D) to achieve the NHPI oxidation transformation to PINO radical, which can further induce the photocatalytic activation of C–H bonds. While the catalytic results do not all comply with the above conjecture. Therefore, combined with the reaction results, discussion about the band gap, and UV-Vis characterization of the metal oxide and oxide/NHPI systems, there should be more detailed reasons for the success of the metal oxides/NHPI shown in Fig. 1A and reasons for other unsuccessful systems. At least, it was conjectured that the appropriate absorption [5] or contaction [7] between NHPI and solid semiconductor surface is the prerequisite factor that cannot be ignored, which allows the further redox process with electron or charge transfer between the NHPI and solid semiconductor.

Table 1

The UV-Vis absorption differences of oxide and oxide/NHPI systems at 455 nm[a].

Entry	Metal Oxide	Band Gap (eV)	Absorption Coefficient without NHPI	Absorption Coefficient with NHPI	Absorption Change Ratio (%) [b]	Photoactivity with NHPI
1	MnO_2	0.25	0.9897	0.9955	0.6	Y
2	CuO	1.70	0.9948	0.9969	0.2	Y
3	Co_3O_4	1.90	0.9634	0.9631	0.0	Y
4	Sb_2O_3	2.20	0.6131	0.6277	2.4	Y
5	Mn_3O_4	2.13	0.9658	0.9695	0.4	N
6	α-Fe_2O_3	2.20	0.9825	0.9890	0.7	Y
7	Cu_2O	2.20	0.9388	0.9798	4.4	N
8	CdO	2.20	0.9956	0.9989	0.3	N
9	WO_3	2.70	0.1991	0.2309	15.9	N[d]
10	CeO_2	2.76	0.2908	0.8294	185.3	N
11	V_2O_5	2.80	0.9960	0.9967	0.1	N
12	PbO	2.80	0.1543	0.4944	220.5	Y
13	Bi_2O_3	2.80	0.2194	0.2744	25.0	Y
14	In_2O_3	2.80	0.2274	0.3534	55.4	N
15	MoO_3	2.94	0.5018	0.5268	5.0	N
16	TiO_2-R	3.20	0.0018	0.0734	3932.9	Y
17	TiO_2-A	3.20	0.0204	0.2126	940.6	Y
18	ZnO	3.20	0.1168	0.7542	545.5	N
19	Al_2O_3	3.21	-0.0192	0.5758	obvious[c]	N
20	Nb_2O_5	3.40	-0.1927	0.1417	obvious	Y
21	Cr_2O_3	3.50	0.9245	0.9553	3.3	N
22	NiO	3.50	0.9547	0.9862	3.3	N
23	SnO_2	3.66	0.6876	0.6887	0.2	N
24	Ta_2O_5	4.00	0.8323	0.9113	9.5	Y
25	Eu_2O_3	4.40	0.7816	0.8787	12.4	N
26	Ga_2O_3	4.80	-0.0064	0.0599	obvious	Y
27	Y_2O_3	4.90	-0.0151	0.0758	obvious	N
28	ZrO_2	5.00	-0.0089	0.0531	obvious	N
29	La_2O_3	5.50	-0.00401	0.0935	obvious	N
30	HfO_2	5.53	0.5557	0.5494	-1.1	N
31	MgO	> 7	-0.0164	0.2695	obvious	N

Note: (a) UV-Vis Data (Fig. S2-S31) have been normalized based on the highest peak between 400 and 800 nm; (b) Absorption change ratio (%) is obtained by the difference between the absorption coefficients with/without NHPI; (c) If the absorption coefficient is changed from negative to positive, it is marked as obvious; (d) The promotion of NHPI on WO_3 photoactivity is not obvious.

3.3. Confirming the mechanism of photocatalytic systems with inhibiting experiments

For the oxides MnO_2, CuO, and Co_3O_4 with the obvious thermal catalytic ability and narrow band gap, besides the photocatalytic process, the redox-metal catalyzed thermal reaction cannot be ignored. For the oxides with obvious blue LEDs and visible light absorption (Sb_2O_3, Fe_2O_3, PbO, and Bi_2O_3), the mechanisms could be mainly attributed to the first NHPI oxidation to PINO radical by the photo-generated h^+ or active O* after the O_2 activation with photo-generated e^-. For the oxides with a band gap beyond the LED light energy (TiO_2, Nb_2O_5, Ta_2O_5, and Ga_2O_3), according to previous reports [32,41], besides the visible light activity caused by structure defect, the combination of metal oxide with NHPI containing an N atom can be regarded as organic doping of the
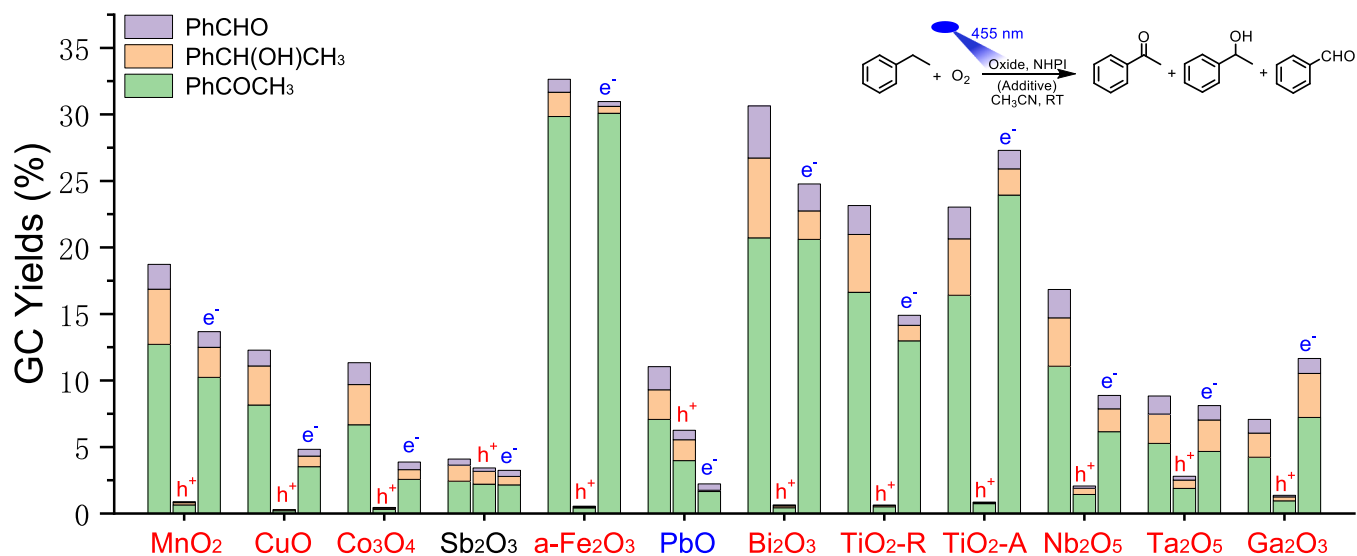

Fig. 2. Photocatalytic ethylbenzene oxidation with different inhibitors. Reaction condition: metal oxide 10 mg, ethylbenzene 0.1 mmol, NHPI 3 mg, acetonitrile 1.0 mL, O_2 1 atom, blue LED light (455 nm, 6 W), additive (0.1 mmol), 30–35 °C, 4 h. The $(NH_4)_2C_2O_4$ is used as the inhibitor for the hole (reactions marked with red h^+), and $AgNO_3$ is used to consume the photo-generated electron (reactions marked with blue e^-).

semiconductor. Otherwise, it is more likely that NHPI molecules act as adsorbed photosensitizers to cooperate with oxides with a wide band gap [35]. Although the NHPI cannot absorb blue light well, the NHPI* adsorbed on the metal oxide may occur structure change and the combination of oxide/NHPI can absorb the blue LEDs (Table 1). Then, these inferences were first checked by the inhibiting experiments. The inhibiting experiments with $(NH_4)_2C_2O_4$ as the scavenger for the light-induced holes (h^+) and $AgNO_3$ as the electron (e^-) scavenger first

indicated the existence of photocatalysis over MnO_2, CuO, and Co_3O_4 with NHPI (Fig. 2). Although the three oxides perform obvious thermal catalysis with NHPI, the hole of these semiconductors with a narrow band gap played a critical role in photocatalysis. For the other listed metal oxides in Fig. 2, besides the Sb_2O_3 without obvious inhibiting effect and PbO with an obvious electron inhibiting effect, the α-Fe_2O_3, Bi_2O_3 with intrinsic visible light absorption ability showed the hole inhibiting effect, and TiO_2, Nb_2O_5 Ta_2O_5, Ga_2O_5 with band gaps beyond
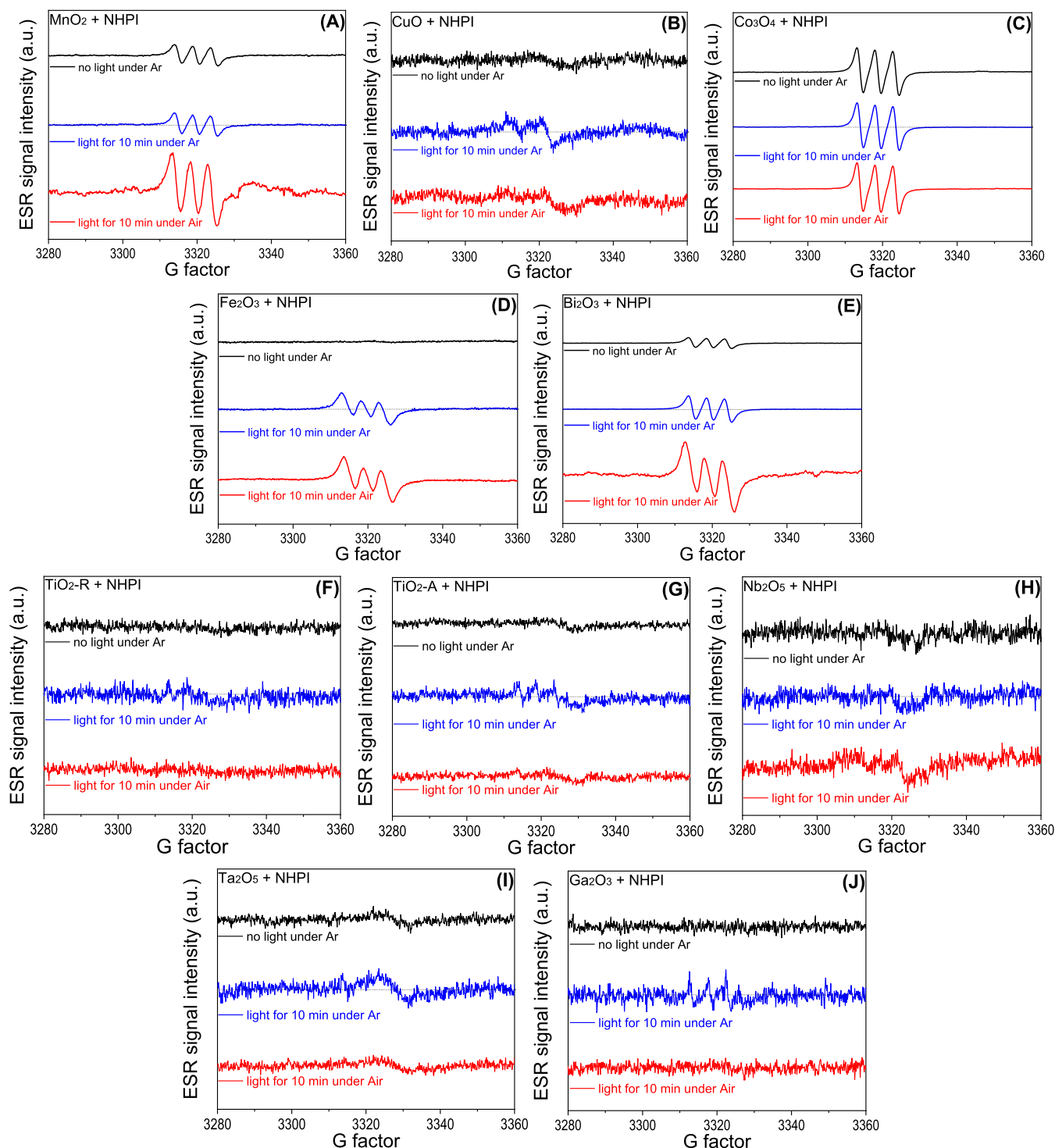

Fig. 3. EPR measurements of metal oxide/NHPI systems. Notes: The mixture of metal oxide 10 mg, NHPI 3 mg, in 1.0 mL CH_3CN after ultrasonic dispersion was injected into the capillary in the EPR tube, which was then tested in Ar atmosphere and dark (a), Ar atmosphere (b) or, air condition (c) with 455 nm blue LED light for 10 min.

the visible light region also showed the inhibiting effect of hole or oxidizing species that associates with the adsorbed NHPI.

3.4. Confirming mechanism of photocatalytic systems with electron paramagnetic resonance (EPR) and photocurrent response (PCR) characterizations

To further confirm the effect of the hole or oxidizing species that associates with the adsorbed NHPI in the photocatalytic oxidation of ethylbenzene (Fig. 2), EPR characterizations were carried out. According to the results in Fig. 1, the PINO radical generated from NHPI is the critical species for the C–H bond HAT activation. If the photo-generated hole plays a critical role in the generation of PINO radical from NHPI, the EPR spectrometer may confirm the signal of PINO radical, which also needs to have an intrinsic long enough lifetime over the metal oxide/NHPI systems under the blue LED irradiation [5,9,42]. As shown in Fig. 3, the combinations in Fig. 2 with the obvious characterization of the h^+-mediated photooxidation were tested, which can be further divided into three kinds: (a) obvious thermal-motivated oxidation generation of N-oxyl radical from NHPI over MnO_2 (Fig. 3A), Co_3O_4 (Fig. 3C), Bi_2O_3 (Fig. 3E), and the potential CuO (Fig. 3B); (b) non-thermal but photo-hole induced N-oxyl radical generation from NHPI over Fe_2O_3 (Fig. 3D), TiO_2-A (Fig. 3G), and Ga_2O_3 (Fig. 3J); (c) unobvious thermal or photo-generated N-oxyl radical generation over the rutile TiO_2-R (Fig. 3F), Nb_2O_5 (Fig. 3H) and Ta_2O_5 (Fig. 3I) at room temperature.

As discussed above, obvious thermal redox oxidation can keep the concentration of PINO radical, which can disturb the confirmation of the N-oxyl generation mechanism induced by the photo-generated hole under blue light irradiation. In addition, the excessively short lifetime of some N-oxyl radicals could be the main reason why their EPR signal is not detected. To confirm the photooxidation mechanism, besides directly capturing the N-oxyl radical EPR signal, the indirect characterization of the corresponding charge transfer via the photocurrent

response (PCR) under the Ar atmosphere was another experimental choice. As the basic principle of PCR testing, light irradiation can cause charge separation over the semiconductor, and then the anode can consume the photo-generated electron, and the left photo-generated hole can undergo annihilation or be reduced by the sacrifice agent. The PCR intensity depends on the intrinsic charge separation efficiency of the semiconductor, but the extra sacrifice agent can accelerate the consumption of the hole and thus increase the PCR intensity. As shown in Fig. 4, the addition of NHPI as the sacrifice agent can obviously increase the photocurrent of the photoanodes of oxides CuO, TiO_2-R, TiO_2-A, Nb_2O_5, Ta_2O_5, and Ga_2O_3, which further confirmed that the photo-generated hole played a critical role over the corresponding semiconductors for the NHPI molecules transformation to the N-oxyl radicals, or the blue light can induce the electron or charge transfer from the absorbed NHPI molecule to the semiconductors.

3.5. Confirming lattice-molecular structure matching effect for the metal/NHPI systems with FTIR characterizations, control experiments, and dynamic analysis

The PCR experiment shows that charge separation will occur in most oxide semiconductors under light irradiation even without NHPI. Although NHPI can be used as a potential hole-consuming reagent because these oxides almost have a high VB potential, not all metal oxide/NHPI systems are capable of C–H bond photocatalytic activation (Fig. 1). Considering the homogeneous-heterogeneous hybrid characteristic of the metal oxide/NHPI system [5], NHPI molecules need to first collide or combine effectively with the oxide semiconductor in an h^+-electron separation state to complete the charge transfer from NHPI molecule to oxide, forming PINO radical to motivate the subsequent HAT process. During this process, there are probably structural matching requirement beyond the energy matching requirement between the oxide semiconductor and NHPI for the photooxidation. Because of the unique adsorption-activation of NHPI molecule on certain metal oxides
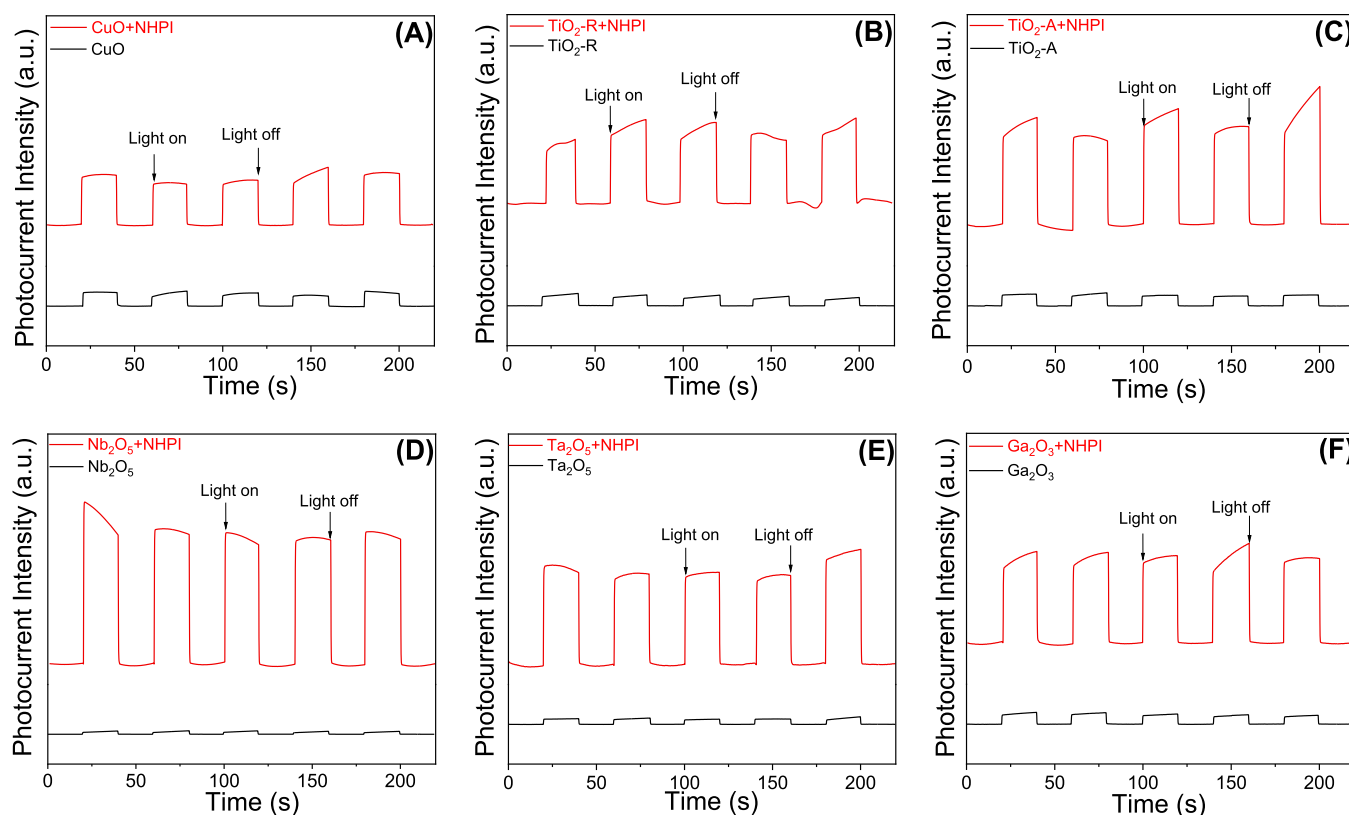

Fig. 4. PCR measurements of metal oxide, and metal oxide/NHPI systems.

(CuO, α-Fe$_2$O$_3$, TiO$_2$-R, TiO$_2$-A, Nb$_2$O$_5$, Ta$_2$O$_5$, and Ga$_2$O$_3$, Fig. 1), and the former lattice-molecular structure matching effect seems to be the basis of the following energy matching effect with NHPI photooxidation to PINO radical over the metal oxides, which may partly explain the unsuccessful of the listed NHPI/oxide systems with metal oxide having a high-enough VB potential.

To prove this conjecture, the α-Fe$_2$O$_3$/NHPI with obvious photocatalysis but negligible thermal catalysis (Fig. 1) in C–H bond activation is an appropriate system. With α-Fe$_2$O$_3$ (0001) face as the lattice surface model, one of the four typical NHPI* adsorption models, vertical (Fig. 4A), push-up (Fig. 4B), side-lying (Fig. 4C), and vacancy (Fig. 4D, giving the existence of vacancy sites on some metal oxides surface [43]), may exist on the surface of various metal oxides. For the dominative state of the NHPI over the α-Fe$_2$O$_3$, the FTIR characterization was carried out (Fig. 4E). The apparent redshift of C=O vibration from 1711 cm^{-1} of free NHPI to 1681 cm^{-1} of adsorbed NHPI indicates the interaction between the two carbonyl groups and the α-Fe$_2$O$_3$ surface. In addition, the new appearance of 1526–1585 cm^{-1} peaks and the red-shift of aromatic ring skeleton vibration (1485 cm^{-1} to 1467 cm^{-1}; 1466 cm^{-1} to 1446 cm^{-1}) suggest the adsorption of the NHPI aromatic ring on the α-Fe$_2$O$_3$ surface. Referring to the basic geometry principle that three points determine one face, the planar molecule NHPI prefers to lie down on the α-Fe$_2$O$_3$ surface with a push-up model (Fig. 4B). In addition, the FTIR peak redshift suggests the charge deflection from the α-Fe$_2$O$_3$ surface to the adsorbed NHPI molecule, which is contrary to the following NHPI photooxidation by the hole of α-Fe$_2$O$_3$. Besides the FTIR peaks red shift of NHPI over the α-Fe$_2$O$_3$, the interaction between the NHPI molecule and the metal oxides listed in Fig. 2 with obvious h$^+$ oxidation characterization were also checked by the FTIR (Table 2 and Fig. S33-S41), which all showed the redshift of the carbonyl group of NHPI. In either case, the FTIR characterization indicates the potential lattice-molecular structure matching requirement for the photocatalysis of metal/NHPI systems.

To further confirm the critical importance of the R$_2$NO–H molecule adsorption on the oxide surface for the photocatalysis of the R$_2$NO–H/metal oxide systems, the photooxidation activities of R$_2$NO–H/metal oxide combinations by using variously structured R$_2$NO–H but fixed the α-Fe$_2$O$_3$ lattice surfaces as the example were checked. As shown in Fig. 5, the molecular structure of the R$_2$NO–H, including the aromatic ring and the 5-atom amide ring, played a critical effect on the photoactivity of R$_2$NO–H/α-Fe$_2$O$_3$ systems, even the existence of the subtle difference in the BDE of various R$_2$NO–H bonds (NHPI 368.4 kJ·mol^{-1} [44], NHSI 362.9 kJ·mol^{-1} [45], NHNI 375.5 kJ·mol^{-1} [44], NDHPI 355.6 kJ·mol^{-1} [44], NHQI, NHCI or HPPDO 369.6 $\pm$ 2.5 kJ·mol^{-1} [46]). The NHPI showed the best photocatalysis with α-Fe$_2$O$_3$, but slight changes by removing the benzene ring (NHPI→NHSI) or replacing the benzene ring with a naphthalene ring and increasing the 5-atom amide ring to the six-atom one (NHPI→NHNI) can restrain the photoactivity. In addition, although the benzene ring and 5-atom amide ring are kept in the NDHPI molecule like NHPI, compressing two NHPI molecules into one NDHPI molecule by introducing the extra 5-atom amide ring on the other side may affect the interaction between R$_2$NO–H and α-Fe$_2$O$_3$, which

Table 2
FTIR spectra of various NHPI/Metal Oxide[a].

Entry	Metal oxide	C=O Zone Change	Benzene Zone Change
1	MnO$_2$	Redshift 71 cm^{-1}	Unobvious
2	CuO	Redshift 72 cm^{-1}	New peaks
3	Co$_3$O$_4$	Redshift 71 cm^{-1}	New peaks and RS[b]
4	Bi$_2$O$_3$	Redshift 22 cm^{-1}	New peaks and RS[b]
5	TiO$_2$-R	Redshift 72 cm^{-1}	Unobvious
6	TiO$_2$-A	Redshift 69 cm^{-1}	New peaks
7	Nb$_2$O$_5$	Redshift 69 cm^{-1}	New peaks
8	Ta$_2$O$_5$	Redshift 37 cm^{-1}	New peaks
9	Ga$_2$O$_3$	Redshift 68 cm^{-1}	New peaks and RS[b]

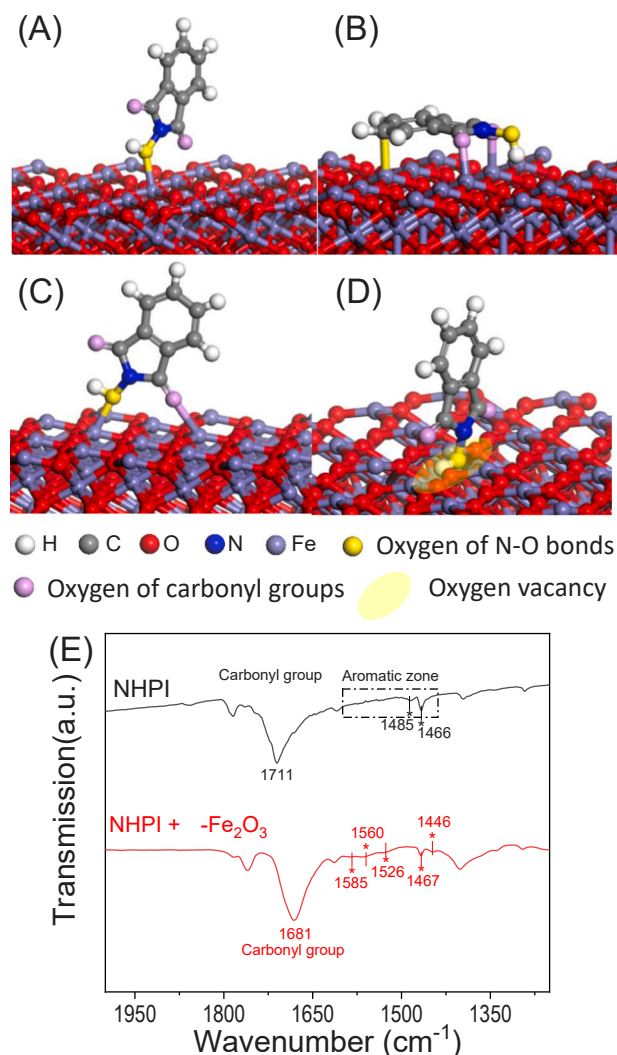Note: (a) FTIR spectra Fig. S33-S41; (b) RS, redshift > 5 cm^{-1}.

Fig. 5. Proposed vertical (A), push-up (B), side-lying (C), and vacancy (D) adsorption models for NHPI* on the surface of semiconductor (with typical α-Fe$_2$O$_3$ (0001) as the sample) and the FTIR spectra of NHPI and NHPI* on the α-Fe$_2$O$_3$ (E).

decrease the photocatalysis. Furthermore, replacing the benzene ring with a pyridine (NHPI→NHQI or NHCI) or pyrazine ring (NHPI→HPPDO) can decrease or restrain the photocatalysis, which could be attributed to the fact that the electron-withdrawing but nucleophilic pyridine or pyrazine could restrain the electron transfer between the organic R$_2$NOH and metal oxide and cause the competitive adsorption of R$_2$NOH on the α-Fe$_2$O$_3$ surface via different atom sites/-zones (like in the pyridine infrared spectrum) to disturb the efficient photocatalysis, referring to the FTIR spectrum and redshift of NHPI on α-Fe$_2$O$_3$ (Fig. 4).

The above photocatalytic results of R$_2$NOH/metal oxide systems with fixed α-Fe$_2$O$_3$ (Fig. 5), combing with the photocatalysis difference presented in Fig. 1 by fixing the R$_2$NO–H molecule NHPI but changing the metal oxides or even fixing the α-Fe$_2$O$_3$ but after different surface treatments (Fig. S42), indicate that there is a lattice-molecular structure matching effect between the R$_2$NO–H molecule and metal oxide semiconductor for this homogeneous/heterogeneous hybrid photocatalysis system, something like putting Legos together. The matching effect as the precondition of the efficient hybrid photocatalytic system needs the R$_2$NO–H molecular structure containing the appropriate atom or organic group sites to precisely anchor it on the oxide lattice surface, which is different from the random absorption. However, the lattice-molecular

structure matching is not the simple Legos piling up, because photo-catalysis requires charge transfer between the organic R$_2$NO–H and the solid oxide semiconductor, and precisely anchoring [5,10,47] can ensure the existence of the potential and efficient charge transfer channel.

3.6. The conjectural mechanism models for the various metal oxide/NHPI combinations

For the potential mechanism of various metal oxide/NHPI combinations, besides the redox metal model, during which the redox metal sites of oxides directly induce the transformation of NHPI to PINO radical and the reduced metal site can be further oxidized back with O$_2$, and the direct C–H substrate oxidation by the hole of the semiconductor like WO$_3$, referring to the results obtained above and previous reports, three potential mechanisms for the photocatalysis of R$_2$NOH/metal oxide systems with the key N-oxyl radical were provide: (1) The electron reduction model (Fig. 6A) [25], the O$_2$ combines with the photo-generated electron (e$^-$) of metal oxides like PbO to the active O*, which then oxidizes NHPI to PINO; (2) The hole oxidation model [5], the photo-generated hole (h$^+$) of metal oxides like α-Fe$_2$O$_3$ directly oxidize the adsorbed or confined NHPI* to PINO (Fig. 6B); (3) Ligand-to-metal charge transfer (LMCT) model (Fig. 6C) [48], the NHPI adsorbs on the metal oxide surface to a combined system, then the light induces the electron transfer from adsorbed NHPI* to the oxide and provides an absorbed or confined PINO*. The ligand-to-metal charge transfer model is somewhat like the photosensitizer mechanism but different, because the NHPI cannot be efficiently activated by the blue LEDs (455 nm), which must be first anchored on the metal oxides like TiO$_2$, Nb$_2$O$_5$, Ta$_2$O$_5$, and Ga$_2$O$_3$ with a wide band gap beyond the energy of the 455 nm LED photon. In addition, the adsorption of NHPI with an N atom can be regarded as the N-doping [7] which may introduce a new

absorption band in the visible light region for the semiconductor with a band gap beyond the visible light region, therefore the visible light irradiation can induce the generation of photo-electron and hole for the O$_2$ activation and following C–H bond activation (Fig. 6C).

3.7. Kinetic characterization of the confined N-oxyl radical over the typical NHPI/α-Fe$_2$O$_3$ system

Furthermore, besides the photocatalysis mechanisms study, we also paid attention to the detailed generation mechanism of confined PINO* radical, especially via the hole oxidation or ligand-to-metal charge transfer mechanism, and the kinetic characterization of the confined N-oxyl radical was preliminarily studied to reveal its difference from the free N-oxyl radical.

For the cleavage of the R$_2$NO–H bond with some certain acidity, adding some base like the typical 2,6-lutidine can first transform the free R$_2$NO–H to the anion R$_2$NO$^-$, which can make the further N-oxyl radical generation in some thermal- and electro- catalysis more easily or with a lower potential than the direct oxidation cleavage of R$_2$NO–H bond. Therefore, for the photocatalytic transform of the NHPI to PINO radical over the metal oxide semiconductors, the homolysis–oxidation process or proton-coupled electron transfer (PCET) [49] process (Scheme 2) may exist given the acid-base property and the photo-induced redox property of various metal oxides. However, in the photocatalytic transformation of adsorbed NHPI* to the PINO* at the surface of photo-activated metal oxides discussed above via the hole oxidation or ligand-to-metal charge transfer mechanism, the control experiment results with 2,6-lutidine as the typical PCET-promoted base failed to accelerate the reaction and even restrain the reaction (Table S1), which indicates the homolysis–oxidation process should be the main mechanism for the N-oxyl radical generation via the photocatalysis over the metal oxide. For the contrary result between the traditional homogeneous-NHPI or PINO system and this hybrid NHPI/oxide system, it could be attributed that the anion R$_2$NO$^-$ may change the absorption state of the original NHPI* because of the stronger nucleophilicity of oxygen-terminal in R$_2$NO$^-$ anion than the one of R$_2$NOH molecule, which partly enhances the conclusion that the appropriate absorption of the NHPI molecule on the metal oxide surface is the key for the photocatalysis of NHPI/metal oxide systems.

As discussed above, the confined N-oxyl radical (PINO*) in this photocatalytic oxidation is a little different from the free PINO radical. To further prove the oxidation is caused by the confined PINO* on the surface of certain metal oxides, the reaction order of NHPI for the photooxidation of ethylbenzene over the typical α-Fe$_2$O$_3$ was checked, which was observed that could generate the typical confined PINO
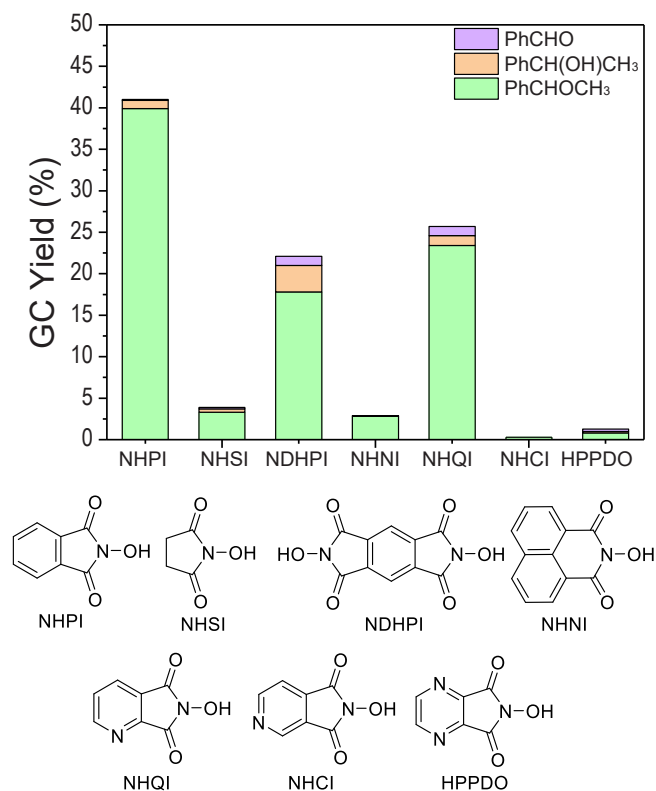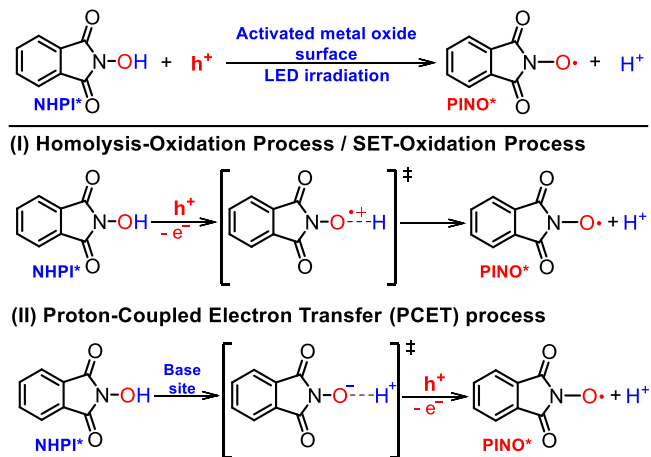

Fig. 6. The photooxidation activities of various R$_2$NO–H/α-Fe$_2$O$_3$ combinations. Reaction conditions: α-Fe$_2$O$_3$ 10 mg, ethylbenzene 0.1 mmol, R$_2$NOH 20 mol% according to the N–OH structure, CH$_3$CN 1.0 mL, O$_2$ 1 atm, blue LED light (455 nm, 18 W), 30–35 °C, 4 h.

Scheme 2. Two mechanisms for the transformation of adsorbed NHPI* to a confined PINO* over the oxide surface.

radical and presented the high activity for C–H HAT activation in our previous work [5]. As shown in Fig. 7, the kinetic data from the oxidation of $PhCH_2CH_3$ over $\alpha\text{-}Fe_2O_3$/NHPI presents a strange "First → Zero → First order" model, which is quite different from the free PINO radical in systems like $Fe(NO_3)_3$/NHPI with a first order of NHPI [30, 50]. To explain this phenomenon, a mechanism with NHPI concentration change was proposed based on previous reports (more discussion in Fig. S43) [5]. As shown in Fig. 8, when the NHPI concentration is lower than 0.024 M, the main process could be caused by the confined PINO* , and the amount of active and confined PINO* working as the HAT centers increases along with the addition of NHPI, which present a first order. Then, the utilization of h^+ centers to promote the generation of the PINO* from NHPI* on the $\alpha\text{-}Fe_2O_3$ surface reaches the saturation state, and the reaction order of NHPI becomes zero order. Further increasing the concentration (> 0.035 M), the extra NHPI can absorb on the $\alpha\text{-}Fe_2O_3$ surface and affect the further transformation of $PhCH(OO\bullet)$ CH_3 or $PhCH(OOH)CH_3$ to ketone with the assistance of solid $\alpha\text{-}Fe_2O_3$ surface (Scheme S4) [19], which can lead to the accumulation of these two intermediates. According to the previous reports, the extra $PhCH(OO\bullet)CH_3$ in liquid phase at a certain concentration may trigger the generation of free PINO radical. In this zone, the free NHPI (Process II of Fig. 8) should have a first order. Given the first order of confined PINO* , zero order of the inactive NHPI* on $\alpha\text{-}Fe_2O_3$ surface, and first order of free PINO radical, the reaction order of NHPI for the ethylbenzene photooxidation at high concentration of NHPI tends to the first order. The kinetic data analysis shows this conjecture may be reasonable (Fig. 8). Therefore, the photooxidation of ethylbenzene catalyzed by the $\alpha\text{-}Fe_2O_3$/NHPI at low NHPI concentration was mainly induced by the confined PINO* radicals on the surface of $\alpha\text{-}Fe_2O_3$. Furthermore, the slope of the fitting curve after the zero-order zone (cNHPI > 0.035) is more obvious than the front zone (cNHPI< 0.025), which may show the difference in generation rate or activity between free PINO and confined PINO* radicals from NHPIFig. 9.

In addition, given the optimized model of NHPI/PINO on the $\alpha\text{-}Fe_2O_3$ surface with a push-up model (Figs. 4B and 4E) and the oxygen terminal is the critical HAT group, the extra confinement effect [5] may decrease the HAT ability of the confined PINO* to activate the C–H substrate with a high steric hindrance, such as the triphenylmethane. As an extension, the triphenylmethane photooxidation was used as another probe reaction to test the activity of PINO* over the metal oxide/NHPI systems listed in Fig. 2 with obvious hole oxidation or ligand-to-metal charge transfer mechanism (Table S2), besides the CuO/NHPI system provided obvious triphenylmethane thermal conversion, other combinations all showed low or unobvious activity. Furthermore, according to the previous report [5], the appropriate confinement can increase the lifetime of the PINO* radical to hundred seconds, which was quite different from free PINO radical with a millisecond time scale lifetime [51,52]. Referring to the FT-IR results (Table 2), the adsorption states of the NHPI over various metal oxides are different, and the strength of the adsorption will be also different at the same time, leading to the various PINO* states, which may partly explain the different EPR spectra of the PINO radical signals (Fig. 3). Nonetheless, the existence of such
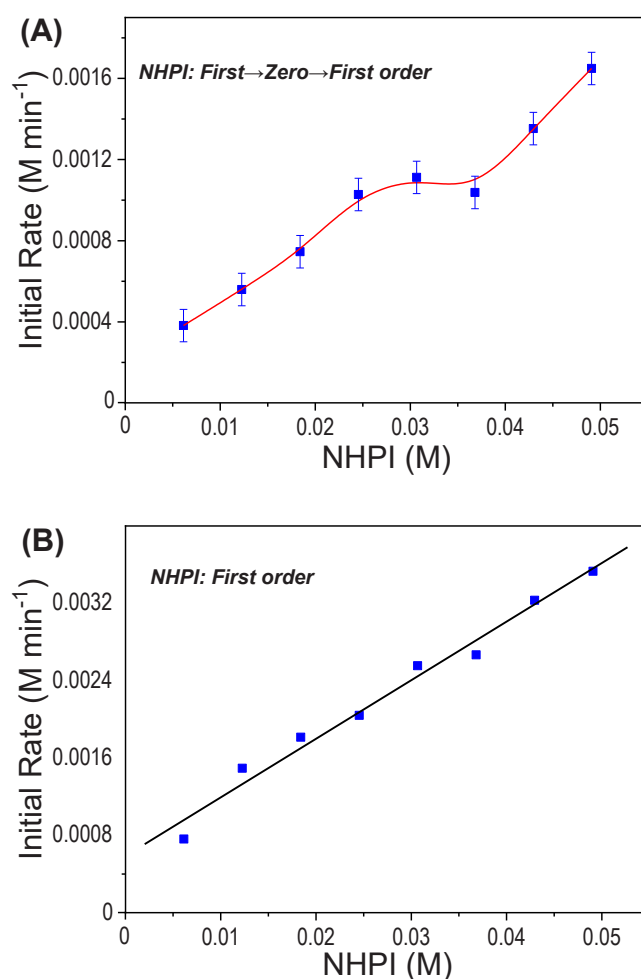
Fig. 8. Kinetic data from the oxidation of $PhCH_2CH_3$ over $\alpha\text{-}Fe_2O_3$/NHPI (A) and $Fe(NO_3)_3$/NHPI (B). Rates were obtained by monitoring ethylbenzene concentration changes. Standard reaction conditions: (A) $PhCH_2CH_3$ 0.5 mmol, 1.0 mL MeCN, 3 atm O_2, $\alpha\text{-}Fe_2O_3$ 10 mg, blue LED light (455 nm, 18 W), 35 °C, 30 min (B) $PhCH_2CH_3$ 0.5 mmol, $Fe(NO_3)_3\cdot9\,H_2O$ 20 mg, 1.0 mL MeCN, 3 atm O_2, no light, 35 °C, 30 min.

differences suggests the possibility to modulate the activity of N-oxyl radicals, which could provide guidance for further optimization of the NHPI/semiconductor systems.

4. Conclusions

In conclusion, to regulate the electric structure of heterogeneous photocatalysts for C–H bond activation, besides incorporating with another semiconductor to build a heterojunction or introducing defect
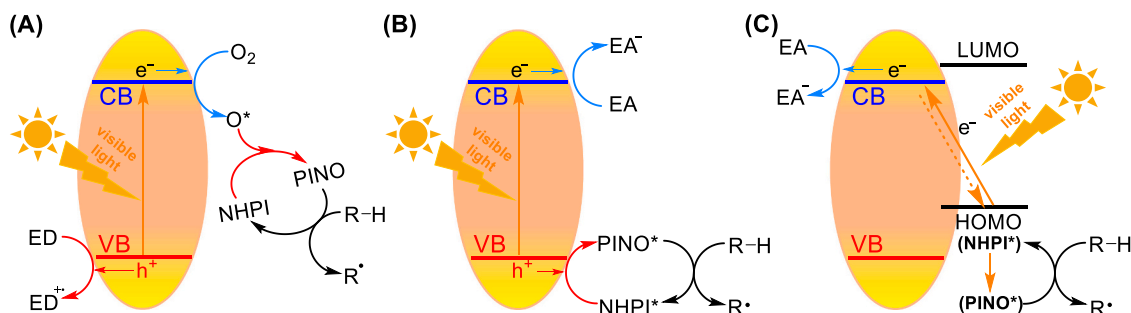
Fig. 7. Conjectural mechanism models for the photocatalysis of metal oxide/NHPI systems. Notes: ED means electron donor; EA means electron acceptor.
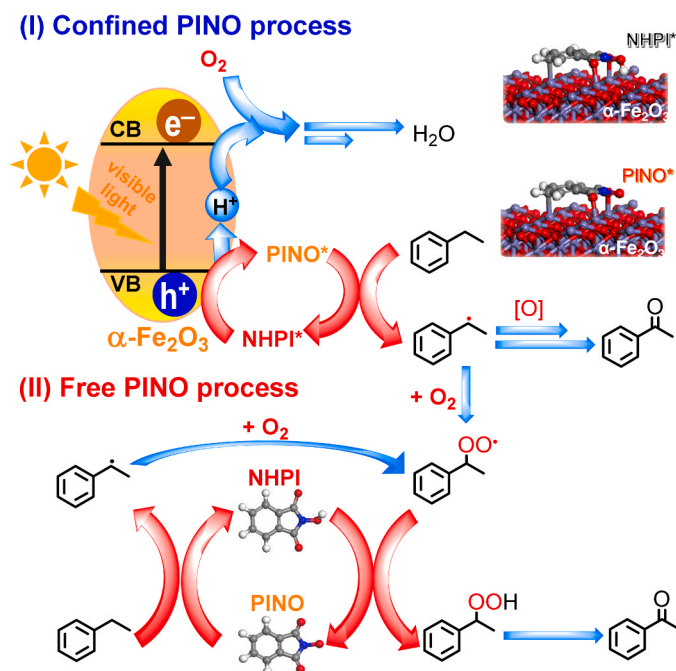
(I) Confined PINO process

(II) Free PINO process

Fig. 9. The mechanism of ethylbenzene oxidation over the α-Fe$_2$O$_3$/NHPI system involving a typical confined N-oxyl radical process (I) and free N-oxyl radical process (II).

level via structure modifying, matching the surface of metal oxide surface with appropriate R$_2$NOH/R$_2$NO$\bullet$ seems another convenient and promising way to enhance the photocatalysis of metal oxides. In this work, the promotion effect of conjugated N-hydroxyphthalimide (NHPI) or phthalimide-N-oxyl radical (PINO) on the photocatalytic C(sp^3)–H bond activation over various metal oxides was systemically checked with control experiments, UV-Vis, FTIR, ESR, and PCR. Three typical photocatalytic mechanism models were proposed to explain the generation of PINO radical over various metal oxides under the blue LEDs irradiation: (1) The electron reduction model; (2) The hole oxidation model; (3) Ligand-to-metal charge transfer (LMCT) model. Furthermore, a lattice-molecular structure matching effect hypothesis, including the structure matching between NHPI molecule and surface lattice of oxide semiconductors, was proposed to explain the success of certain oxides in building the h$^+$ oxidation systems or ligand-to-metal charge transfer systems with NHPI. In addition, the kinetic characterization of the confined N-oxyl radical was preliminarily studied to reveal its difference from the free N-oxyl radical. The corresponding results can inspire further photocatalysis of semiconductors in C–H bond activation with versatile N-oxyl radicals.

CRediT authorship contribution statement

Ting Li: Methodology, Validation, Resources, Data curation, Visualization. **Kaiyi Su:** Methodology, Software, Formal analysis, Writing - review & editing. **Chaofeng Zhang:** Conceptualization, Methodology, Investigation, Project administration, Supervision, Writing - original draft, Writing - review & editing, and Funding acquisition. **Bingbing Luo:** Resources, Data curation. **Yue Zhang:** Resources, Data Curation. **Jinlan Cheng:** Visualization, Supervision, and Writing - review & editing. **Yongcan Jin:** Supervision, Writing - review & editing. **Feng Wang:** Conceptualization, Writing - review & editing.

Declaration of Competing Interest

The authors declare that they have no known competing financial interests or personal relationships that could have appeared to influence

the work reported in this paper.

Data availability

Data will be made available on request.

Appendix A. Supporting information

Supplementary data associated with this article can be found in the online version at doi:10.1016/j.apcatb.2023.123432.

References

[1] A.A. Fokin, P.R. Schreiner, Selective alkane transformations via radicals and radical cations: insights into the activation step from experiment and theory, Chem. Rev. 102 (2002) 1551–1593.

[2] S.S. Stahl, Chemistry. Palladium-catalyzed oxidation of organic chemicals with O$_2$, Science 309 (2005) 1824–1826.

[3] L. Chen, J. Tang, L.-N. Song, P. Chen, J. He, C.-T. Au, S.-F. Yin, Heterogeneous photocatalysis for selective oxidation of alcohols and hydrocarbons, Appl. Catal., B 242 (2019) 379–388.

[4] J.E. Nutting, M. Rafiee, S.S. Stahl, Tetramethylpiperidine N-Oxyl (TEMPO), Phthalimide N-Oxyl (PINO), and Related N-Oxyl species: electrochemical properties and their use in electrocatalytic reactions, Chem. Rev. 118 (2018) 4834–4885.

[5] C. Zhang, Z. Huang, J. Lu, N. Luo, F. Wang, Generation and confinement of long-lived N-oxyl radical and its photocatalysis, J. Am. Chem. Soc. 140 (2018) 2032–2035.

[6] W.-L. He, C.-D. Wu, Incorporation of Fe-phthalocyanines into a porous organic framework for highly efficient photocatalytic oxidation of arylalkanes, Appl. Catal., B 234 (2018) 290–295.

[7] H. Hao, J.-L. Shi, H. Xu, X. Li, X. Lang, N-hydroxyphthalimide-TiO$_2$ complex visible light photocatalysis, Appl. Catal., B 246 (2019) 149–155.

[8] Y. Bian, Y. Gu, X. Zhang, H. Chen, Z. Li, Engineering BiOBr$_{1-x}$ solid solutions with enhanced singlet oxygen production for photocatalytic benzylic C–H bond activation mediated by N-hydroxyl compounds, Chin. Chem. Lett. 32 (2021) 2837–2840.

[9] K. Su, C. Zhang, Y. Wang, J. Zhang, Q. Guo, Z. Gao, F. Wang, Unveiling the highly disordered NbO$_6$ units as electron-transfer sites in Nb$_2$O$_5$ photocatalysis with N-hydroxyphthalimide under visible light irradiation, Chin. J. Catal. 43 (2022) 1894–1905.

[10] M. Tamura, E. Sagawa, A. Nakayama, Y. Nakagawa, K. Tomishige, Hydrogen atom abstraction by heterogeneous–homogeneous hybrid catalyst of CeO$_2$ and 2-cyanopyridine via redox of CeO$_2$ for C–H bond oxidation with air, ACS Catal. 11 (2021) 11867–11872.

[11] J. Zhou, X. Li, X. Ma, W. Sheng, X. Lang, Cooperative photocatalysis of dye-TiO$_2$ nanotubes with TEMPO$^+$BF$_4^-$ for selective aerobic oxidation of amines driven by green light, 120368, Appl. Catal., B 296 (2021) 120368.

[12] X. Li, S. Yang, F. Zhang, L. Zheng, X. Lang, Facile synthesis of 2D covalent organic frameworks for cooperative photocatalysis with TEMPO: The selective aerobic oxidation of benzyl amines, Appl. Catal., B 303 (2022) 120846.

[13] J. Kong, F. Zhang, C. Zhang, W. Chang, L. Liu, J. Li, An efficient electrochemical oxidation of C(sp^3)-H bond for the synthesis of arylketones, Mol. Catal. 530 (2022) 112633.

[14] F.R. Mayo, Free-radical autoxidations of hydrocarbons, Acc. Chem. Res. 1 (1968) 193–201.

[15] C. Schweitzer, R. Schmidt, Physical mechanisms of generation and deactivation of singlet oxygen, Chem. Rev. 103 (2003) 1685–1757.

[16] Y. Nosaka, A.Y. Nosaka, Generation and detection of reactive oxygen species in photocatalysis, Chem. Rev. 117 (2017) 11302–11336.

[17] N. Gupta, B.A. Baraiya, P.K. Jha, H.P. Soni, Differentiating the {100} surfaces of Cu$_2$O nanocrystals from {111} and {110} for benzylic Csp^3-H bond oxidation: Oxidations of diphenyl methane to benzophenone and cumene to cumene hydroperoxide under mild conditions, Mol. Catal. 528 (2022) 112490.

[18] Y. Ishii, S. Sakaguchi, T. Iwahama, Innovation of hydrocarbon oxidation with molecular oxygen and related reactions, Adv. Synth. Catal. 343 (2001) 393–427.

[19] G.Y. Yang, Y.F. Ma, J. Xu, Biomimetic catalytic system driven by electron transfer for selective oxygenation of hydrocarbon, J. Am. Chem. Soc. 126 (2004) 10542–10543.

[20] M.B. Lauber, S.S. Stahl, Efficient aerobic oxidation of secondary alcohols at ambient temperature with an ABNO/NO$_x$ catalyst system, ACS Catal. 3 (2013) 2612–2616.

[21] Y.P. Yan, P. Feng, Q.Z. Zheng, Y.F. Liang, J.F. Lu, Y.X. Cui, N. Jiao, PdCl$_2$ and N-hydroxyphthalimide co-catalyzed C(sp^2)-H hydroxylation by dioxygen activation, Angew. Chem. -Int. Ed. 52 (2013) 5827–5831.

[22] F. Recupero, C. Punta, Free radical functionalization of organic compounds catalyzed by N-hydroxyphthalimide, Chem. Rev. 107 (2007) 3800–3842.

[23] L.P. Zhou, C.F. Zhang, T. Fang, B.B. Zhang, Y. Wang, X.M. Yang, W. Zhang, J. Xu, Selective Oxidation of Alcohols Catalyzed by a Transition Metal-Free System of NHPI/DDQ/NaNO$_2$, Chin. J. Catal. 32 (2011) 118–122.

[24] C. Zhang, H. Li, J. Lu, X. Zhang, K.E. MacArthur, M. Heggen, F. Wang, Promoting lignin depolymerization and restraining the condensation via an oxidation−hydrogenation strategy, ACS Catal. 7 (2017) 3419–3429.

[25] P. Zhang, Y. Wang, J. Yao, C. Wang, C. Yan, M. Antonietti, H. Li, Visible-light-induced metal-free allylic oxidation utilizing a coupled photocatalytic system of g-C$_3$N$_4$ and N-hydroxy compounds, Adv. Synth. Catal. 353 (2011) 1447–1451.

[26] M. Rafiee, K.C. Miles, S.S. Stahl, Electrocatalytic alcohol oxidation with TEMPO and bicyclic nitroxyl derivatives: driving force trumps steric effects, J. Am. Chem. Soc. 137 (2015) 14751–14757.

[27] A. Badalyan, S.S. Stahl, Cooperative electrocatalytic alcohol oxidation with electron-proton-transfer mediators, Nature 535 (2016) 406–410.

[28] J. Luo, J. Zhang, Aerobic oxidation of olefins and lignin model compounds using photogenerated phthalimide-N-oxyl radical, J. Org. Chem. 81 (2016) 9131–9137.

[29] E. Baciocchi, M. Bietti, M. Di Fusco, O. Lanzalunga, D. Raponi, Electron-transfer properties of short-lived N-oxyl radicals. Kinetic study of the reactions of benzotriazole-N-oxyl radicals with ferrocenes. Comparison with the phthalimide-N-oxyl radical, J. Org. Chem. 74 (2009) 5576–5583.

[30] M. Mazzonna, M. Bietti, G.A. DiLabio, O. Lanzalunga, M. Salamone, Importance of π-stacking interactions in the hydrogen atom transfer reactions from activated phenols to short-lived N-oxyl radicals, J. Org. Chem. 79 (2014) 5209–5218.

[31] B.L. Ryland, S.D. McCann, T.C. Brunold, S.S. Stahl, Mechanism of alcohol oxidation mediated by copper(II) and nitroxyl radicals, J. Am. Chem. Soc. 136 (2014) 12166–12173.

[32] S. Furukawa, Y. Ohno, T. Shishido, K. Teramura, T. Tanaka, Selective amine oxidation using Nb$_2$O$_5$ photocatalyst and O$_2$, ACS Catal. 1 (2011) 1150–1153.

[33] H.J. Chen, C. Liu, M. Wang, C.F. Zhang, N.C. Luo, Y.H. Wang, H. Abroshan, G. Li, F. Wang, Visible light gold nanocluster photocatalyst: selective aerobic oxidation of amines to imines, ACS Catal. 7 (2017) 3632–3638.

[34] S. Zavahir, Q. Xiao, S. Sarina, J. Zhao, S. Bottle, M. Wellard, J.F. Jia, L.Q. Jing, Y. M. Huang, J.P. Blinco, H.S. Wu, H.Y. Zhu, Selective oxidation of aliphatic alcohols using molecular oxygen at ambient temperature: mixed-valence vanadium oxide photocatalysts, ACS Catal. 6 (2016) 3580–3588.

[35] M. Zhang, C. Chen, W. Ma, J. Zhao, Visible-light-induced aerobic oxidation of alcohols in a coupled photocatalytic system of dye-sensitized TiO$_2$ and TEMPO, Angew. Chem. Int. Ed. 47 (2008) 9730–9733.

[36] D. Ravelli, M. Fagnoni, T. Fukuyama, T. Nishikawa, I. Ryu, Site-selective C–H functionalization by decatungstate anion photocatalysis: synergistic control by polar and steric effects expands the reaction scope, ACS Catal. 8 (2018) 701–713.

[37] S.L. Wei, X.L. Zhu, P.Y. Zhang, Y.Y. Fan, Z.H. Sun, X. Zhao, D.X. Han, L. Niu, Aerobic oxidation of methane to formaldehyde mediated by crystal-O over gold modified tungsten trioxide via photocatalysis, Appl. Catal., B 283 (2021), 119661.

[38] Y. Xu, M.A.A. Schoonen, The absolute energy positions of conduction and valence bands of selected semiconducting minerals, Am. Mineral. 85 (2000) 543–556.

[39] B. Nourozi, A. Aminian, N. Fili, Y. Zangeneh, A. Boochani, P. Darabi, The electronic and optical properties of MgO mono-layer: Based on GGA-mBJ, Results Phys. 12 (2019) 2038–2043.

[40] R. Amorati, M. Lucarini, V. Mugnaini, G.F. Pedulli, F. Minisci, F. Recupero, F. Fontana, P. Astolfi, L. Greci, Hydroxylamines as oxidation catalysts: thermochemical and kinetic studies, J. Org. Chem. 68 (2003) 1747–1754.

[41] S. Furukawa, T. Shishido, K. Teramura, T. Tanaka, Photocatalytic Oxidation of Alcohols over TiO$_2$ Covered with Nb$_2$O$_5$, ACS Catal. 2 (2012) 175–179.

[42] X.-H. Liu, H.-Y. Yu, J.-Y. Huang, X.-T. Zhou, C. Xue, H.-B. Ji, Time-resolved EPR revealed C(sp^3)–H activation through a photo-enhanced phthalimide-N-oxyl (PINO) radical, Chem. Commun 59 (2023) 243–246.

[43] Y. Wang, F. Wang, Q. Song, Q. Xin, S. Xu, J. Xu, Heterogeneous ceria catalyst with water-tolerant Lewis acidic sites for one-pot synthesis of 1,3-diols via Prins condensation and hydrolysis reactions, J. Am. Chem. Soc. 135 (2013) 1506–1515.

[44] K.X. Chen, L. Jia, C.M. Wang, J. Yao, Z.R. Chen, H.R. Li, Theoretical design of multi-nitroxyl organocatalysts with enhanced reactivity for aerobic oxidation, ChemPhysChem 15 (2014) 1673–1680.

[45] K.X. Chen, H.Y. Xie, K.Z. Jiang, J.Y. Mao, Theoretical study on the catalytic reactivity of N-hydroxyphthalimide tuned by different heterocyclic substitutions on its phenyl ring for aerobic oxidation, Chem. Phys. Lett. 657 (2016) 135–141.

[46] G.A. DiLabio, P. Franchi, O. Lanzalunga, A. Lapi, F. Lucarini, M. Lucarini, M. Mazzonna, V.K. Prasad, B. Ticconi, Hydrogen atom transfer (HAT) processes promoted by the quinolinimide-N-oxyl radical. A kinetic and theoretical study, J. Org. Chem. 82 (2017) 6133–6141.

[47] M. Tamura, R. Kishi, A. Nakayama, Y. Nakagawa, J. Hasegawa, K. Tomishige, Formation of a new, strongly basic nitrogen anion by metal oxide modification, J. Am. Chem. Soc. 139 (2017) 11857–11867.

[48] G. Zhang, G. Kim, W. Choi, Visible light driven photocatalysis mediated via ligand-to-metal charge transfer (LMCT): an alternative approach to solar activation of titania, Energy Environ. Sci. 7 (2014) 954.

[49] S. Ghosh, J. Castillo-Lora, A.V. Soudackov, J.M. Mayer, S. Hammes-Schiffer, Theoretical insights into proton-coupled electron transfer from a photoreduced ZnO nanocrystal to an organic radical, Nano Lett. 17 (2017) 5762–5767.

[50] C.X. Miao, H.Q. Zhao, Q.Y. Zhao, C.G. Xia, W. Sun, NHPI and ferric nitrate: a mild and selective system for aerobic oxidation of benzylic methylenes, Catal. Sci. Technol. 6 (2016) 1378–1383.

[51] E. Baciocchi, M. Bietti, C. D'Alfonso, O. Lanzalunga, A. Lapi, M. Salamone, One-electron oxidation of ferrocenes by short-lived N-oxyl radicals. The role of structural effects on the intrinsic electron transfer reactivities, Org. Biomol. Chem. 9 (2011) 4085–4090.

[52] E. Baciocchi, M. Bietti, M. Di Fusco, O. Lanzalunga, A kinetic study of the electron-transfer reaction of the phthalimide-N-oxyl radical (PINO) with ferrocenes, J. Org. Chem. 72 (2007) 8748–8754.